

**Electronic Supplementary Information**

**Sustained Acid Release from Stimuli Responsive Organic Crystals Facilitates  
Shape Modulation in Metal Nanoparticle Synthesis**

Khalid Naim,<sup>a†</sup> Prodipta Samadder,<sup>a†</sup> Atikur Rahman,<sup>a</sup> Subash Chandra Sahoo,<sup>b</sup> Prakash P.

Neelakandan<sup>\*a,c</sup>

<sup>a</sup> Institute of Nano Science and Technology, Sector 81, Mohali 140306, India. Email:  
ppn@inst.ac.in

<sup>b</sup> Department of Chemistry, Panjab University, Sector 14, Chandigarh 160014, India.

<sup>c</sup> Academy of Scientific and Innovative Research (AcSIR), Ghaziabad 201002, India.

<sup>†</sup> Contributed equally.

## EXPERIMENTAL SECTION

### General Techniques

All experiments were carried out at room temperature ( $25 \pm 1$  °C) unless otherwise mentioned. Melting points (m.p.) were measured in open capillaries with a Stuart (automatic melting point SMP50) apparatus and are uncorrected. NMR spectra were measured on a 400 MHz Bruker Avance Neo spectrometer. NMR spectra were internally referenced to residual solvent signal at  $\delta$  7.26 ppm for  $\text{CDCl}_3$ . Hexafluorobenzene was used as the internal standard for  $^{19}\text{F}$  NMR spectra in toluene- $d_8$  and the reference peak position for  $^{19}\text{F}$  was taken as  $\delta$   $-164.9$  ppm.<sup>1</sup> Mass spectra were measured on a Shimadzu gas chromatograph coupled with a GCMS-QP 2010 plus mass detector and a single-quadrupole mass spectrometer Quantum (Shimadzu) with 100% dimethyl polysiloxane (Restek Rxi-1 ms; 30 mm  $\times$  0.25 mm, 0.25  $\mu\text{m}$  film thickness) column. Absorption spectra were recorded on a Shimadzu UV-Vis spectrophotometer in 3 mL quartz cuvettes having a path length of 1 cm. Reflectance spectra of solid samples were measured on Shimadzu UV-2600 UV-Vis spectrophotometer. Fluorescence spectra were recorded on a Fluorolog 3-221 fluorimeter equipped with 450 W Xenon lamp. Fluorescence lifetimes were measured on a Fluorolog TCSPC Horiba FL-1057. Crystals were observed with an optical microscope (Olympus BX53F). Field emission scanning electron microscope (FESEM) images were captured using Jeol JSM-7610FPlus FESEM, and EDX analysis was performed with Z2-i7 analyzer. X-ray photoelectron spectroscopy (XPS) spectra were recorded by using an Al  $K\alpha$  X-ray source (1486.7 eV) and a monochromator with ultrahigh vacuum provided by Thermo Fisher Scientific.

### Single Crystal X-ray analysis

Single crystals suitable for diffraction studies were grown and were mounted on Hampton cryo-loops. All geometric and intensity data for the crystals were collected using a Super-Nova (Mo) X-ray diffractometer equipped with a micro-focus sealed X-ray tube Mo- $K\alpha$  ( $\lambda = 0.71073$  Å) X-ray source, and HyPix3000 detector with increasing  $\omega$  (width of 0.3 per frame) at a scan speed of either 5 or 10 s/frame. The CrysAlisPro software was used for data acquisition and data extraction. Using Olex2,<sup>2</sup> the structure was solved with the SIR2004<sup>3</sup> structure solution program using Direct Methods and refined with the ShelXL<sup>4</sup> refinement package using Least Squares minimization. All non-hydrogen atoms were refined with anisotropic thermal parameters. Detailed crystallographic data and structural refinement parameters are

summarized in Table S1. CCDC 2361379 and 2361403 contains the supplementary crystallographic data. These data can be obtained free of charge from The Cambridge Crystallographic Data Centre.

Hydrogen atom positions were determined using X-ray crystallographic data by employing a combination of statistical analysis and refinement techniques.<sup>5</sup> Initially, H-atoms were placed in calculated positions based on geometrical considerations using standard bond lengths and angles. These positions were refined using the riding model, wherein hydrogen atoms were constrained to move along with their parent atoms while maintaining fixed distances. Isotropic displacement parameters for the hydrogen atoms were set at 1.2–1.5 times the equivalent isotropic displacement parameter ( $U_{eq}$ ) of the bonded non-hydrogen atoms. A difference Fourier map was used to verify the placement of hydrogen atoms, particularly for those involved in hydrogen bonding. Statistical validation of the hydrogen positions was performed by analysing refinement residuals and thermal parameters using ShelXL refinement software.

### **Hirshfeld Analysis**

Important intermolecular interactions within the crystal structure were identified through Hirshfeld surface analysis using Crystal Explorer 17.5.<sup>6</sup> The Hirshfeld surface is defined as a set of points in 3D space where the ratio of promolecule and procrystal electron densities is equal to 0.5.<sup>7</sup> The exploration of intermolecular contacts is provided by mapping normalized contact distances ( $d_{norm}$ ), which is a function of a closest distance from the point to the nuclei interior ( $d_i$ ) and exterior ( $d_e$ ) to the surface as well as on the van der Waals radii ( $r^{vdw}$ ). Hirshfeld surface  $d_{norm}$ , displays various intermolecular interactions in terms of red, blue and white colour scheme, in which red denotes short contacts, white highlights interactions operating within the range of van der Waals radii and blue represent long range contacts. 2D fingerprints were generated by deriving the Hirshfeld surface by plotting the fraction of points on the surface as the function of  $d_i$  and  $d_e$  which provide a visual summary of intermolecular contacts within the crystal.

## Computational Details

Ground state ( $S_0$ ) of different compounds were optimized using density functional theory (DFT) and electronic absorption spectra was calculated using time-dependent density functional theory (TD-DFT) as implemented in Gaussian 09 package program<sup>7</sup>. GaussView 06 was used to visualise optimized structures. Ground state optimization, frequency calculation, Highest Occupied Molecular Orbital (HOMO) and Lowest Unoccupied Molecular Orbital (LUMO) optimization were performed by employing B3LYP exchange functional with 6-31++g(d,p) basis set. On the basis of the Frank-Condon principle, the absorption properties were evaluated using the optimized  $S_0$  state structure.

## Materials

1-Hydroxy-2-naphthaldehyde, 2-hydroxy-1-naphthaldehyde, and N,N-diethyl-*p*-phenylenediamine were purchased from TCI Chemicals. Boron trifluoride diethyletherate was purchased from Sigma-Aldrich. Silica gel (60-120 mesh), methanol, dichloromethane (DCM), hexane, and trimethylamine were purchased locally. Solvents were distilled and dried before use.

## Syntheses

Compounds **1** and **2** were synthesized as reported earlier<sup>8</sup> and their characterization data are presented in Fig. S1-S4.

## Calculation of the difference in dipole moments of ground and excited states<sup>8,9</sup>

According to Lippert-Mataga equation,

$$\bar{\nu}_A - \bar{\nu}_F = \frac{2}{hc} \left( \frac{\varepsilon - 1}{2\varepsilon + 1} - \frac{n^2 - 1}{2n^2 + 1} \right) \frac{(\mu_E - \mu_G)^2}{a^3} + Constant$$

$$\Delta\bar{\nu} = \frac{2\Delta f}{hca^3} \Delta\mu^2 + Constant$$

where  $\bar{\nu}_A - \bar{\nu}_F = \Delta\bar{\nu}$ ,  $\left( \frac{\varepsilon - 1}{2\varepsilon + 1} - \frac{n^2 - 1}{2n^2 + 1} \right) = \Delta f$  and  $(\mu_E - \mu_G)^2 = \Delta\mu^2$ .

$$slope = \frac{2}{hca^3} \Delta\mu^2$$

In the above equation,  $h$  is Planck's constant,  $c$  is the speed of light, and  $a$  is the Onsager cavity radius.  $\bar{\nu}_A$  and  $\bar{\nu}_F$  are the wavenumbers ( $\text{cm}^{-1}$ ) of the absorption and emission bands respectively.  $\Delta\mu = \mu_E - \mu_G$  is the difference between the dipole moments of the excited and the ground states, respectively.  $\varepsilon$  and  $n$  are the dielectric constant and refraction index, respectively, of the solvent, which are grouped in the term  $\Delta f$ , known as orientation polarizability. The Onsager radius was determined from the single-crystal structure, with values of 3.294 and 3.313 Å for compounds **1** and **2**, respectively. It was estimated as half of the average distance between the nitrogen atom (N2) of the diethylamine donor and the boron acceptor atom (B1), representing the longest molecular dimension where charge separation can occur. The difference between the dipole moments of the excited and ground states was calculated using the slope of the Lippert-Mataga plot and the Onsager radius.

### **Protonated crystals**

The crystals of **1H** were grown by the slow vapour diffusion method. 20 mg of **1** was dissolved in 3 mL of DCM in a glass tube and one drop of concentrated HCl was added to this solution. This tube was placed in another glass tube containing 2 mL of hexane. The system was closed and left undisturbed, and upon solvent evaporation crystals of **1H** were obtained.

The crystals of **2H** were grown by a similar method. 12 mg of **2** was dissolved in 3 mL of acetonitrile in a 5 mL glass tube and one drop of concentrated HCl was added to this solution. Then this tube was placed in a 50 mL glass tube that contained 3 mL of diethyl ether. The system was closed and left undisturbed, and upon solvent evaporation crystals of **2H** were obtained.

### **Quantification of acid in 1H and 2H**

**Acid base titration.** To quantify the amount of acid released from the crystals of **1H** and **2H**, an acid-base titration was performed. 13.2 mg of the crystals of **1H** or 9.5 mg of the crystals of **2H** were added to 25 mL of distilled water. The heterogeneous mixture was stirred at 30 °C for 5 hours to ensure complete dissolution of HCl, which was confirmed by the colour and luminescence changes of the residual crystals. The solution was filtered to remove residual crystals, and the crystals were dried at room temperature. The dried crystals were analysed

through  $^1\text{H}$  NMR spectroscopy to confirm the formation of **1**. A few drops of methyl orange indicator was added to the HCl-containing water and was titrated against a solution of  $\text{Na}_2\text{CO}_3$  in water, and the endpoint was identified by a colour change from red to yellow. This titration was repeated in triplicate to ensure accuracy and reproducibility. The molarity and the amount of acid released were calculated using the titration data and the stoichiometric relationship from the balanced chemical equation.

$$V_1 S_1 = 2 V_2 S_2$$

$V_1$  = volume of sodium carbonate solution used.

$S_1$  = concentration of sodium carbonate solution used.

$V_2$  = volume of unknown HCl solution used.

$S_2$  = concentration of unknown HCl solution (to be determined).

### **Kinetic analysis of acid release from 1H and 2H**

Crystals of **1H** and **2H** were placed in a vacuum-sealed, temperature-dependent emission measurement setup in a spectrofluorimeter. The temperature was maintained at 30 °C, and the emission intensity at a specific wavelength (480 nm for **1H** and 542 nm for **2H**) was monitored at regular time intervals. The relative changes in emission intensity were then plotted against time (h), and the data were fitted to obtain the rate constant value from the slope for each step.

### **Nanoparticle synthesis**

**Silver nanocubes.** 1.32 mg of **1H** was added to 5 mL of distilled water in a vial, and the vial was capped and stirred in an oil bath at 30°C for 30 minutes. Then,  $\text{AgNO}_3$  (3 mL from a 94 mM solution in water) and poly(vinyl pyrrolidone) (PVP,  $M_w$  40000 in terms of the repeating unit; 3 mL from a 147 mM solution in water) were simultaneously added at a rate of 45 mL per hour to the stirring solution. Upon the addition of the solution of  $\text{AgNO}_3$ , the reaction mixture went through a series of colour changes that included milky white, light yellow, transparent, red, and ochre. After the reaction, the residual crystals were filtered out and the solution was washed with acetone and water to remove excess PVP and  $\text{AgNO}_3$ . Characterization of the nanocubes were performed using scanning electron microscopy (SEM).

**Gold nanotriangles.** The synthesis of gold nanotriangles were carried out similar to that used for silver nanocubes. Specifically, 2 ml of 0.25 mM aqueous hydro chlorauric acid ( $\text{HAuCl}_4 \cdot 3\text{H}_2\text{O}$ ) and 8 mL of 10 mM poly(vinyl pyrrolidone) (PVP;  $M_w$  40000) were simultaneously added at a rate of 40 mL per hour to the stirring solution. The change of pale-yellow solution to light blue solution over 5 hours of reaction indicated the synthesis of gold nanotriangles. After the reaction, the post-synthesis procedure was carried out as mentioned above.

**Table S1.** Photophysical properties of compounds **1**, **2**, **1H** and **2H** in the crystalline state.

Solid	$\lambda_{\text{abs}}$ (nm)	$\lambda_{\text{em}}$ (nm)	$\phi_f$	$\tau_f$ (ns)			$k_r$ (s <sup>-1</sup> )	$k_{nr}$ (s <sup>-1</sup> )
				$\tau_1$	$\tau_2$	$\tau_3$		
<b>1</b>	433	583	12.3±0.0 02	1.44±0.0 3 (33.04%)	3.31±0.0 1 (66.96%)		4.0 x 10 <sup>7</sup>	29.5 x10 <sup>7</sup>
<b>2</b>	463	612	21.6±0.0 05	1.62±0.0 2 (16.48%)	3.81±0.0 1 (83.52%)		4.1 x 10 <sup>7</sup>	23.3 x10 <sup>7</sup>
<b>1H</b>	408	484	6.13±0.0 6	1.10±0.1 0 (11.65%)	2.37±0.0 1 (88.36%)		2.6 x 10 <sup>7</sup>	40.8 x 10 <sup>7</sup>
<b>2H</b>	433	542	4.39±0.0 07	0.89±0.0 3 (30.90%)	2.38±0.0 4 (55.53%)	5.85± 0.11 (13.57 %)	1.1 x 10 <sup>7</sup>	28.7 x10 <sup>7</sup>



**Table S2.** Crystal data and structure refinement parameters for **1**, **2**, **1H** and **2H**.

Compound	<b>1</b>	<b>2</b>	<b>1H</b>	<b>2H</b>
CCDC no.	2003922	2003921	2361379	2361403
Empirical formula	C <sub>21</sub> H <sub>21</sub> BF <sub>2</sub> N <sub>2</sub> O	C <sub>21</sub> H <sub>21</sub> BF <sub>2</sub> N <sub>2</sub> O	C <sub>21</sub> H <sub>22</sub> BClF <sub>2</sub> N <sub>2</sub> O	C <sub>23</sub> H <sub>25</sub> BClF <sub>2</sub> N <sub>3</sub> O
Formula weight	366.23	366.21	402.66	443.72
Temperature/K	293	145.67(14)	293(2)	293(2)
Crystal system	monoclinic	triclinic	monoclinic	orthorhombic
Space group	P2 <sub>1</sub> /c	P $\bar{1}$	P2 <sub>1</sub> /c	Pbca
a/Å	6.5954(4)	6.47630(10)	15.2366(3)	7.7073(3)
b/Å	18.2138(9)	9.6428(3)	11.4016(2)	12.5804(4)
c/Å	15.1647(8)	15.2178(3)	11.5082(2)	46.8762(16)
$\alpha$ /°	90	97.517(2)	90	90
$\beta$ /°	94.405(5)	101.143(2)	95.415(2)	90
$\gamma$ /°	90	100.811(2)	90	90
Volume/Å <sup>3</sup>	1816.31(17)	902.01(4)	1990.30(6)	4545.2(3)
Z	4	2	4	8
$\rho_{\text{calc}}$ /cm <sup>3</sup>	1.3392	1.348	1.344	1.297
$\mu$ /mm <sup>-1</sup>	0.096	0.097	0.224	0.204
F(000)	768.4	384.0	840.0	1856.0
Radiation	Mo K $\alpha$ ( $\lambda$ = 0.71073)	MoK $\alpha$ ( $\lambda$ = 0.71073)	MoK $\alpha$ ( $\lambda$ = 0.71073)	Mo K $\alpha$ ( $\lambda$ = 0.71073)
2 $\theta$ range for data collection/°	6.58 to 54.14	6.434 to 54.862	6.452 to 54.764	6.328 to 54.808
Index ranges	-8 $\leq$ h $\leq$ 8, -22 $\leq$ k $\leq$ 23, -19 $\leq$ l $\leq$ 18	-8 $\leq$ h $\leq$ 8, -11 $\leq$ k $\leq$ 12, -19 $\leq$ l $\leq$ 17	-19 $\leq$ h $\leq$ 19, -14 $\leq$ k $\leq$ 14, -13 $\leq$ l $\leq$ 14	-9 $\leq$ h $\leq$ 9, -16 $\leq$ k $\leq$ 15, -59 $\leq$ l $\leq$ 58
Reflections collected	25107	11066	28305	36567

Independent reflections	3948 [R <sub>int</sub> = 0.0885, R <sub>sigma</sub> = 0.0643]	3803 [R <sub>int</sub> = 0.0340, R <sub>sigma</sub> = 0.0474]	4364 [R <sub>int</sub> = 0.0378, R <sub>sigma</sub> = 0.0237]	4925 [R <sub>int</sub> = 0.0989, R <sub>sigma</sub> = 0.0825]
Data/restraints/parameters	3948/0/245	3803/7/246	4364/0/255	4925/0/283
Goodness-of-fit on F <sup>2</sup>	1.023	1.048	1.099	1.037
Final R indexes [I>=2σ (I)]	R <sub>1</sub> = 0.0535, wR <sub>2</sub> = 0.1461	R <sub>1</sub> = 0.0507, wR <sub>2</sub> = 0.1143	R <sub>1</sub> = 0.0444, wR <sub>2</sub> = 0.1224	R <sub>1</sub> = 0.0720, wR <sub>2</sub> = 0.1860
Final R indexes [all data]	R <sub>1</sub> = 0.0746, wR <sub>2</sub> = 0.1687	R <sub>1</sub> = 0.0728, wR <sub>2</sub> = 0.1287	R <sub>1</sub> = 0.0554, wR <sub>2</sub> = 0.1302	R <sub>1</sub> = 0.1417, wR <sub>2</sub> = 0.2195
Largest diff. peak/hole / e Å <sup>-3</sup>	0.30/-0.33	0.38/-0.23	0.41/-0.27	0.31/-0.33

**Table S3.** Percentage of intermolecular interactions present in **1**, **2**, **1H** and **2H** derived from Hirshfeld surface analysis.

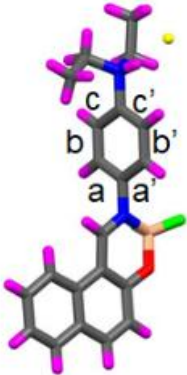
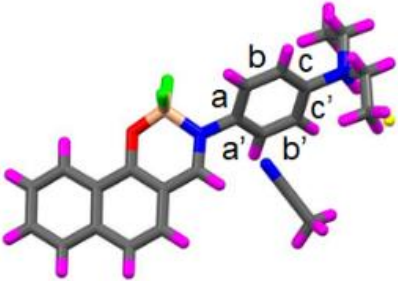
Interactions	<b>1</b>	<b>2</b>
% C...H	30.4	26.2
% C...C	1	4.2
% H...H	43.7	45.3
% N...H	1.6	2
% F...H	16.7	18.5
% O...H	5.2	3.9
$\rho = [(\%C\cdots H)/(\%C\cdots C)]$	30.4	6.23

Interactions	<b>1H</b>	<b>2H</b>
% C...H	19	7.7
% C...C	3.8	6
% H...H	43.4	53.4
% Cl...H	11.3	10.7
% F...O	16.8	-
% O...H	4.3	2.2
% C...O	0.3	1.3
% C...F	0.6	1
% F...H	-	16.5
% C...N	-	0.2
% H...N	-	0.7
$\rho = [(\%C\cdots H)/(\%C\cdots C)]$	5	1.28

**Table S4.** Comparison of quinoid character in the crystals of **1H** and **2H** using the equation

$$\delta_r = \frac{\left[ \frac{(a+a')}{2} - \frac{(b+b')}{2} \right] + \left[ \frac{(c+c')}{2} - \frac{(b+b')}{2} \right]}{2}$$

where a, b and c are bond lengths as depicted below.

Structures		$\delta_r/\text{\AA}$
	a = 1.378, a' = 1.380	-0.005
	b = 1.380, b' = 1.386	
	c = 1.382, c' = 1.371	
	a = 1.393, a' = 1.370	-0.002
	b = 1.375, b' = 1.379	
	c = 1.366, c' = 1.372	

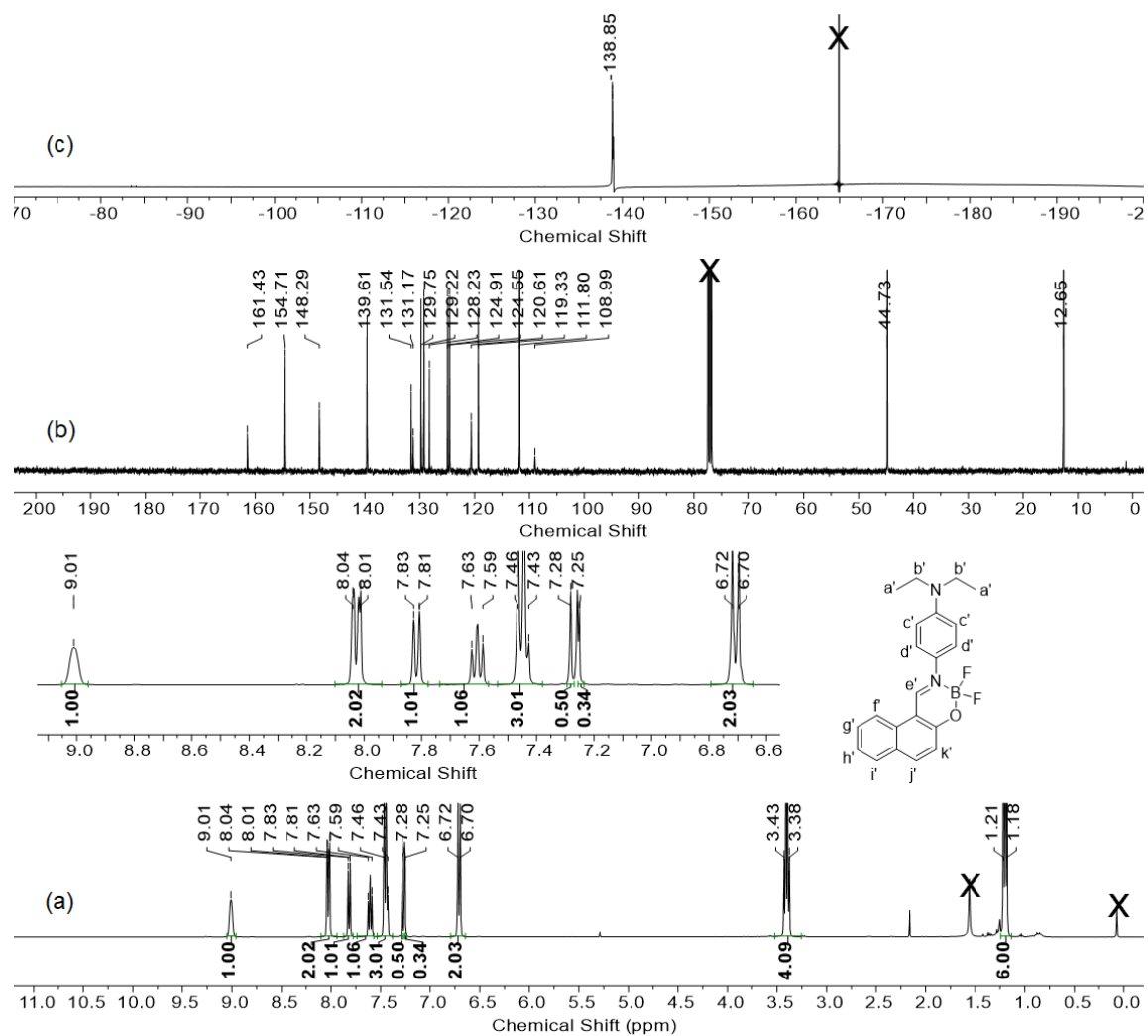


**Fig. S1.** (a)  $^1\text{H}$ , (b)  $^{13}\text{C}$  and (c)  $^{19}\text{F}$  NMR spectra of **1** in  $\text{CDCl}_3$  at 298 K. Inset of (a) shows the region between  $\delta$  6.55 and 9.13 ppm.

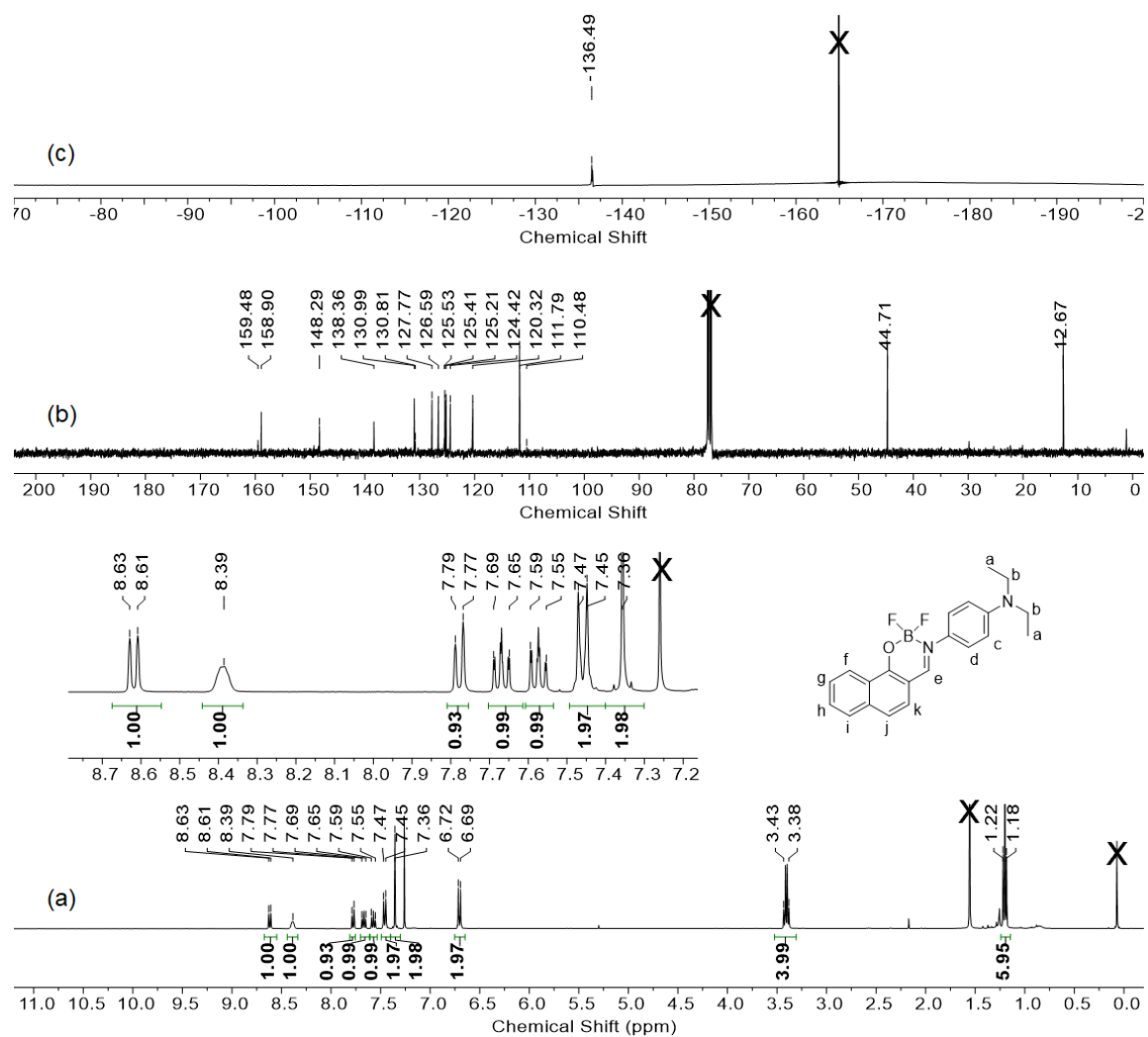


**Fig. S2.** (a)  $^1\text{H}$ , (b)  $^{13}\text{C}$  and (c)  $^{19}\text{F}$  NMR spectra of **2**  $\text{CDCl}_3$  at 298 K. Inset of (a) shows the region between  $\delta$  7.16 and 8.78 ppm.

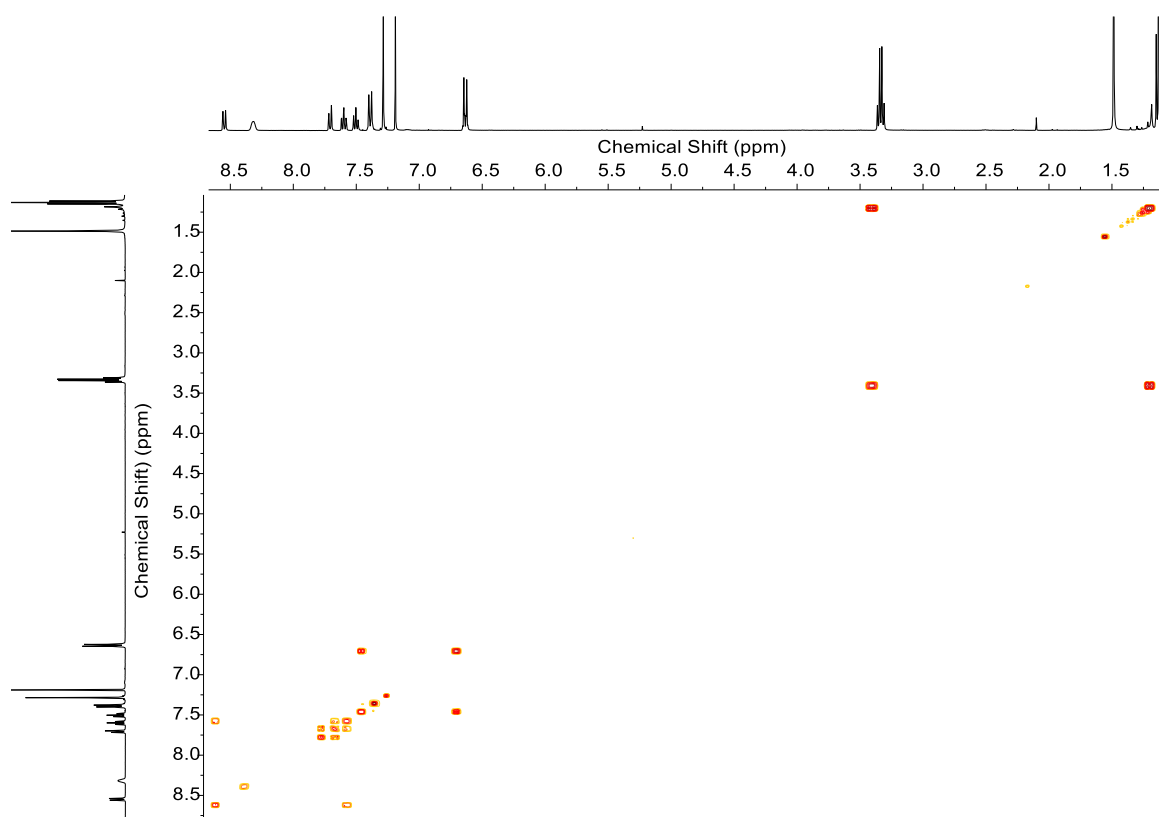


**Fig. S3.**  $^1\text{H}$ - $^1\text{H}$  COSY spectrum of **1** in  $\text{CDCl}_3$ .

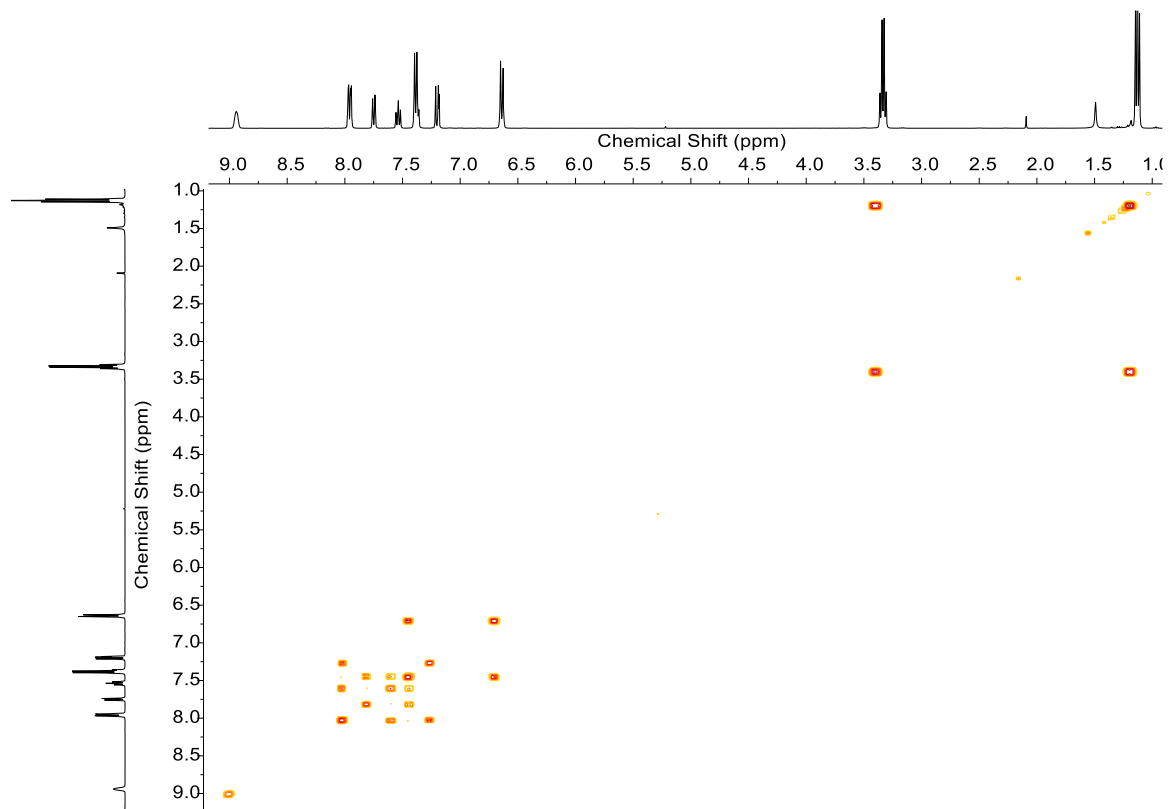


**Fig. S4.**  $^1\text{H}$ - $^1\text{H}$  COSY spectrum of **2** in  $\text{CDCl}_3$ .

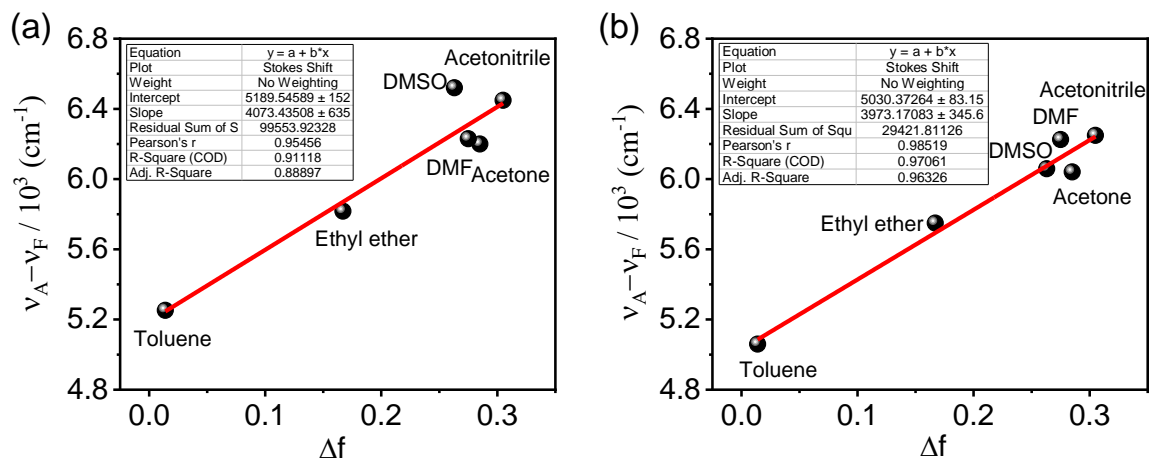


**Fig. S5.** Lippert-Mataga plot of (a) **1** (20  $\mu$ M) and (b) **2** (20  $\mu$ M) in solvents of different polarity.

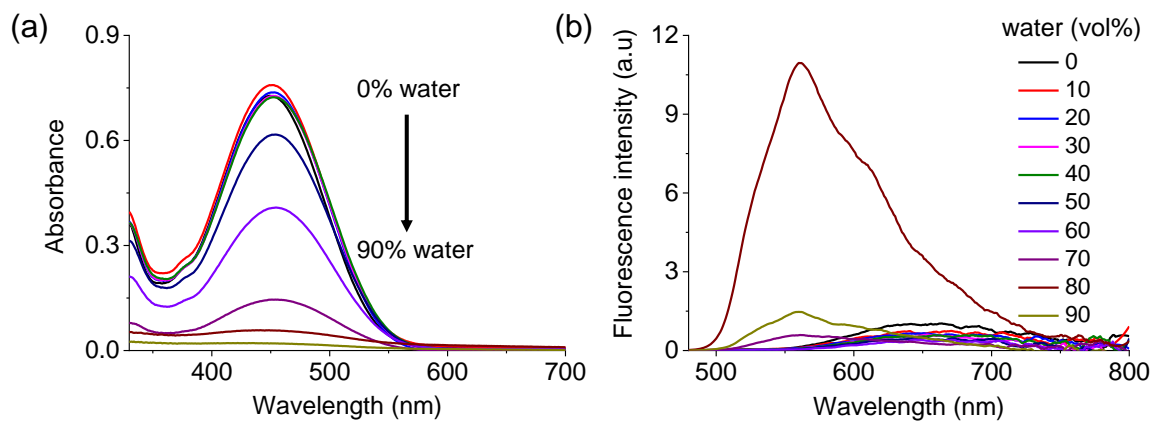


**Fig. S6.** (a) Absorption and (b) emission spectra of **1** (20  $\mu$ M) in acetonitrile-water mixtures.



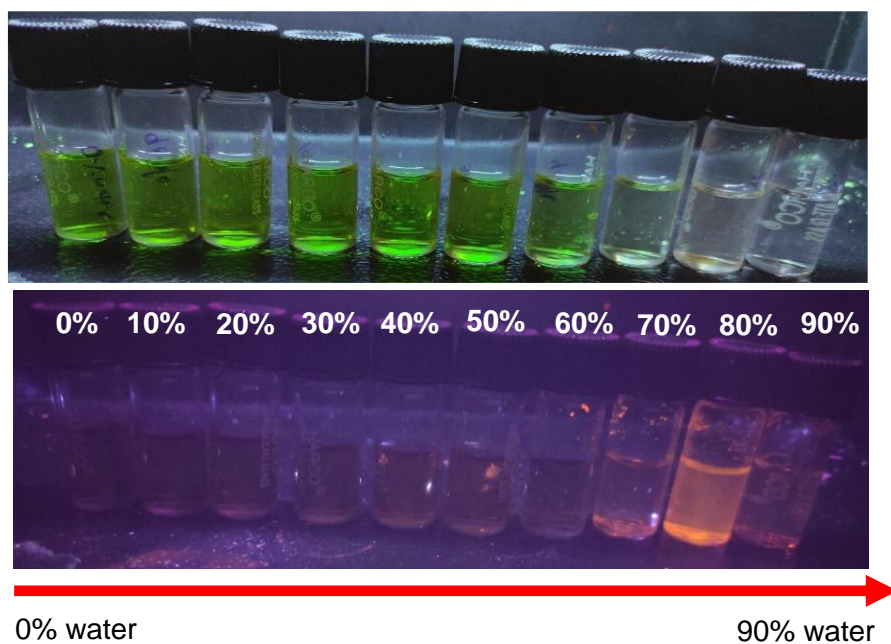


**Fig. S7.** Photographs of **1** (20  $\mu\text{M}$ ) in acetonitrile-water mixtures taken under (a) day light and (b) UV illumination.

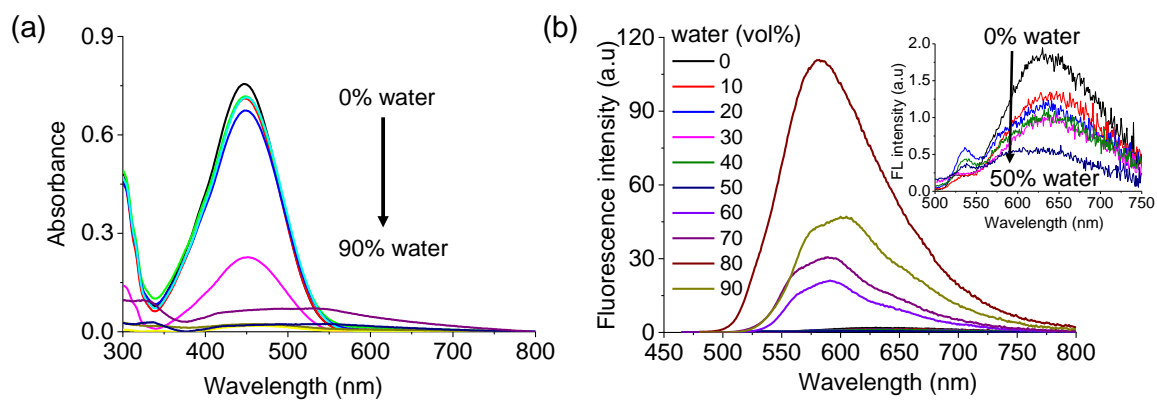


**Fig. S8.** (a) Absorption and (b) emission spectra of **2** (20  $\mu\text{M}$ ) in acetonitrile-water mixtures with different fractions of water. Inset shows the enlarged region from 0 to 2 fluorescence intensity.



**Fig. S9.** Photographs of **2** ( $20\ \mu\text{M}$ ) in acetonitrile-water mixtures with different fractions of water taken under day light and UV illumination.

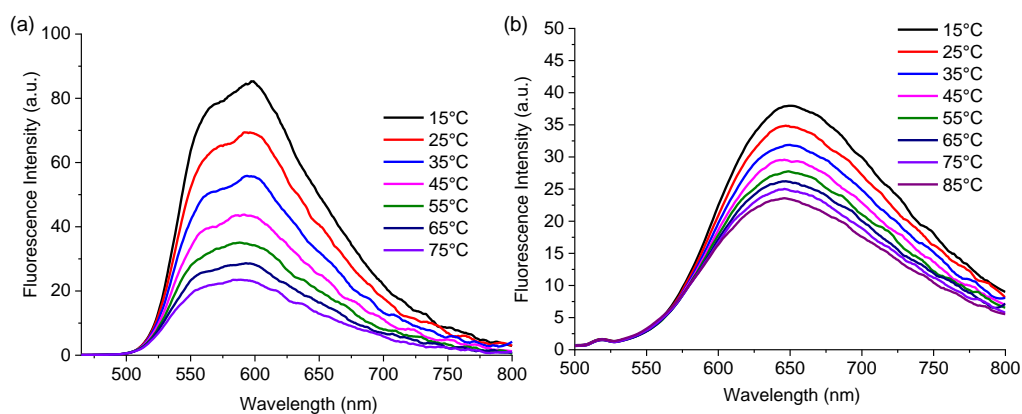


**Fig. S10.** Fluorescence spectra of **1** ( $20\ \mu\text{M}$ ) in (a) toluene and (b) DMF at different temperatures. DMF is dimethylformamide.

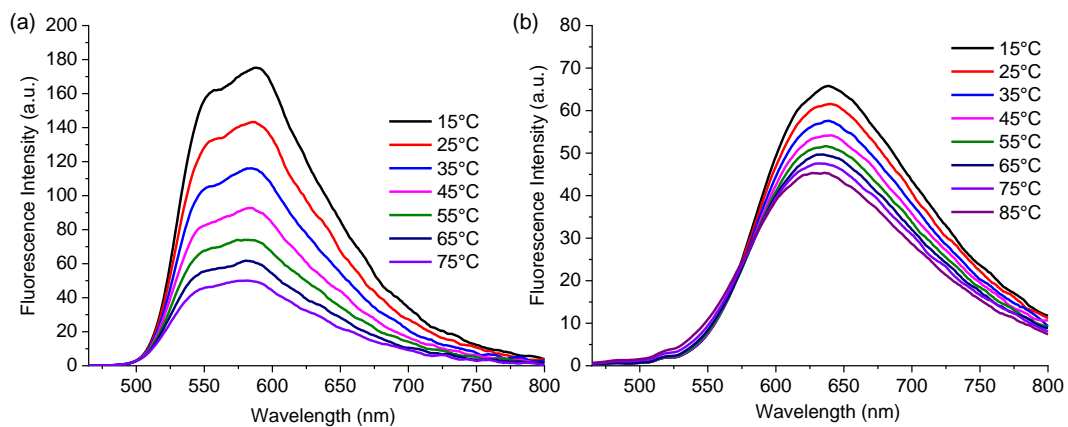


**Fig. S11.** Fluorescence spectra of **2** (20  $\mu\text{M}$ ) in (a) toluene and (b) DMF at different temperatures.

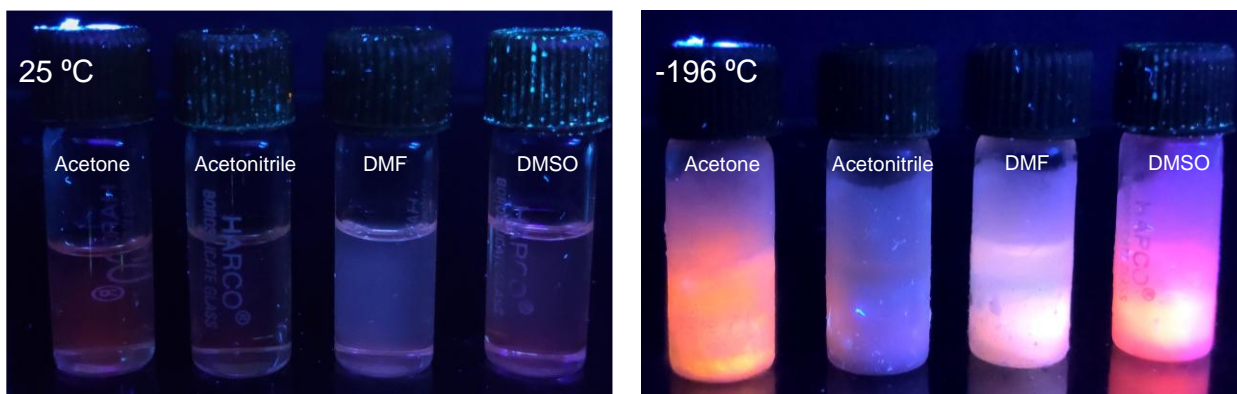


**Fig. S12.** Digital photographs of **1** (20  $\mu\text{M}$ ) in acetone, acetonitrile, DMF and DMSO at 25 and  $-196$   $^{\circ}\text{C}$ .

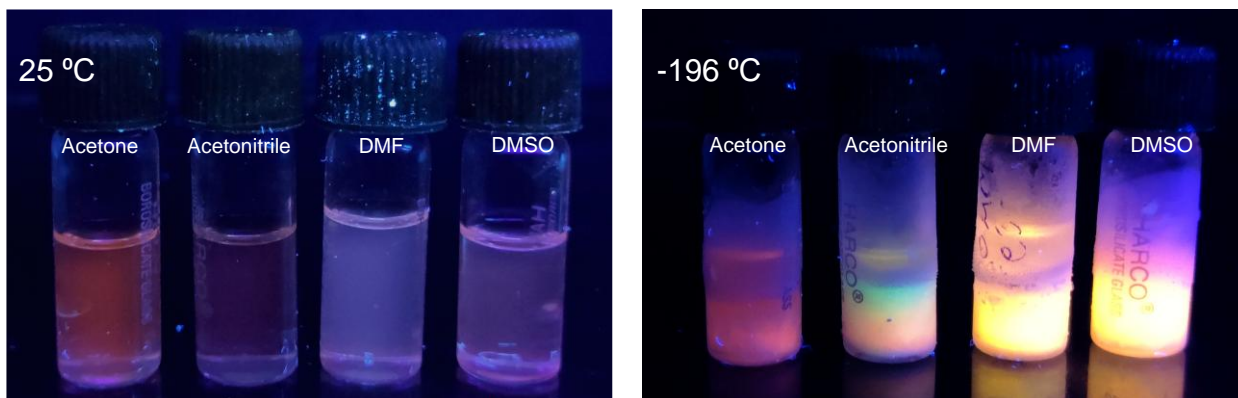


**Fig. S13.** Digital photographs of **2** (20  $\mu\text{M}$ ) in acetone, acetonitrile, DMF and DMSO at 25 and  $-196\text{ }^\circ\text{C}$ .

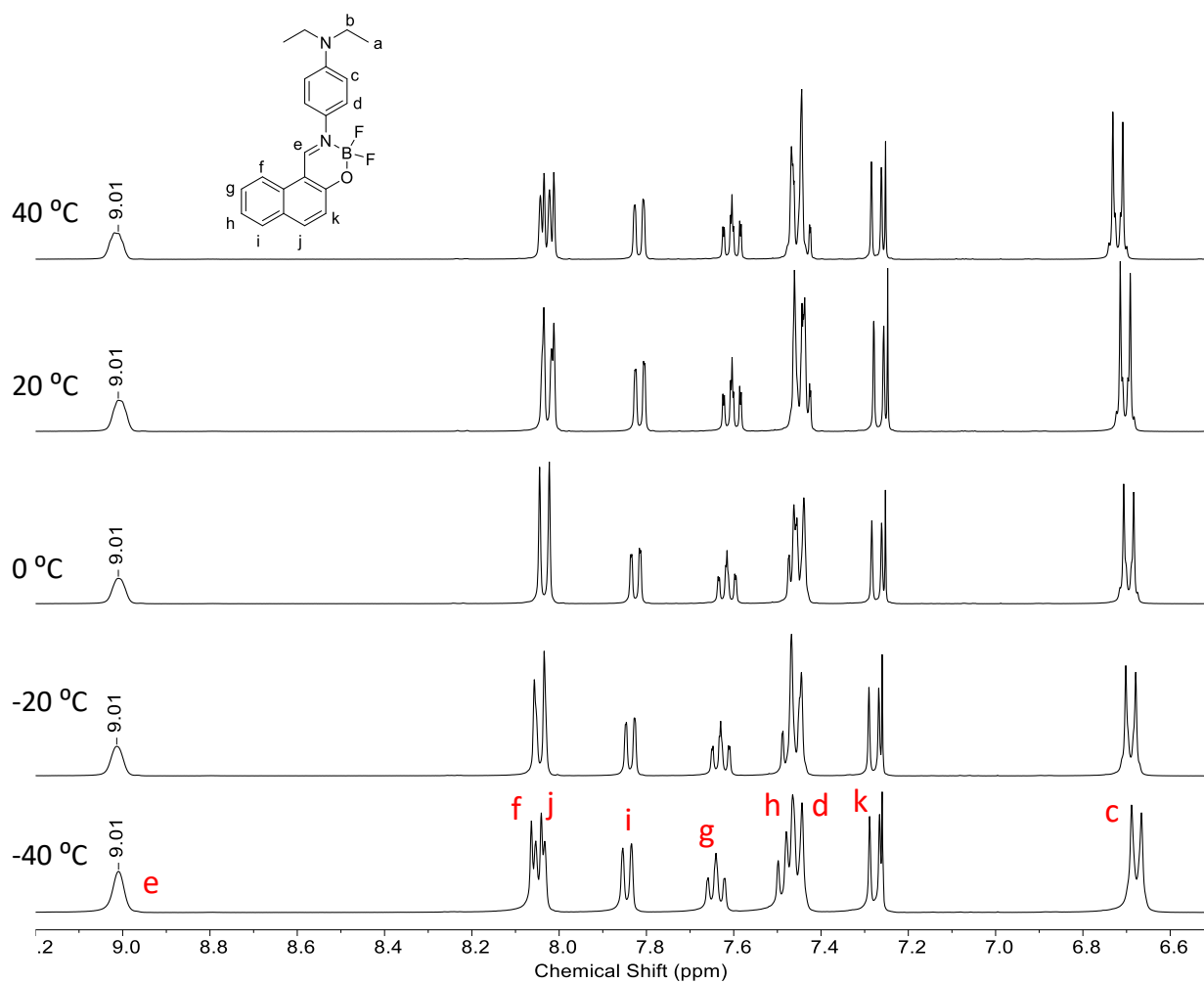


**Fig. S14.**  $^1\text{H}$  NMR spectra of **1** (27.3 mM) in  $\text{CDCl}_3$  at different temperatures.

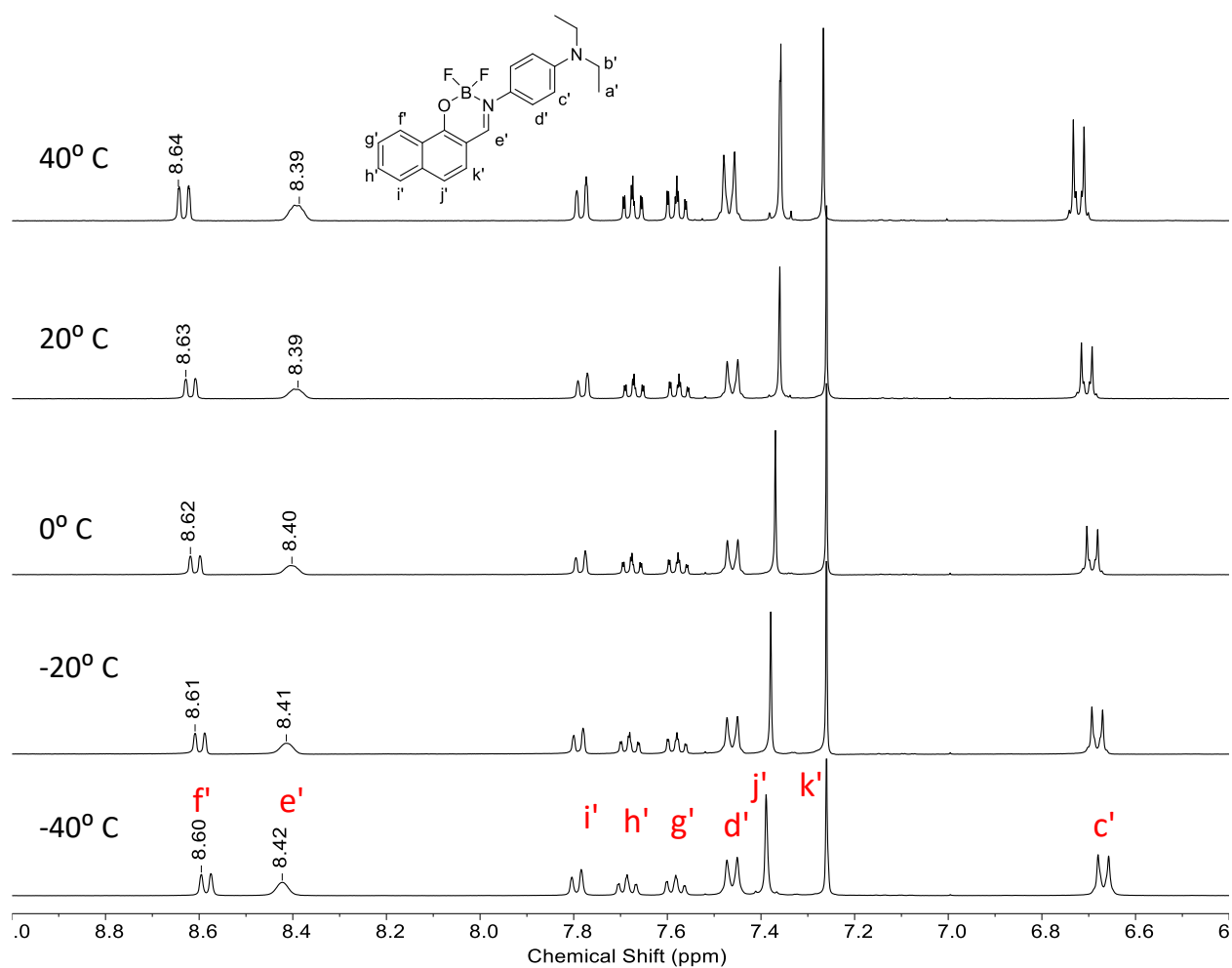


**Fig. S15.**  $^1\text{H}$  NMR spectra of **2** (27.3 mM) in  $\text{CDCl}_3$  at different temperatures.

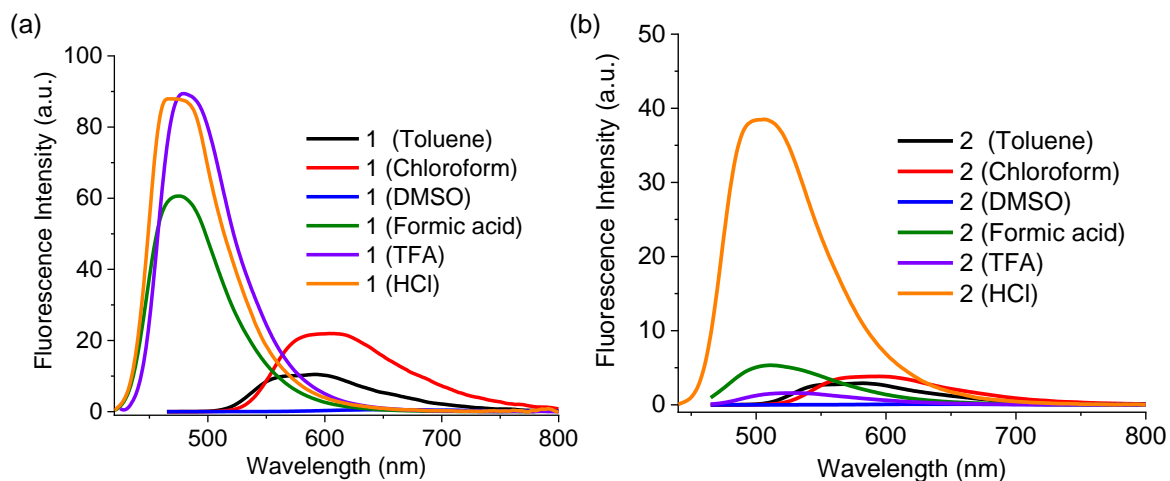


**Fig. S16.** Fluorescence spectra of **1** (20 μM) and **2** (20 μM) in organic solvents (toluene, chloroform, DMSO), formic acid trifluoroacetic acid and hydrochloric acid.

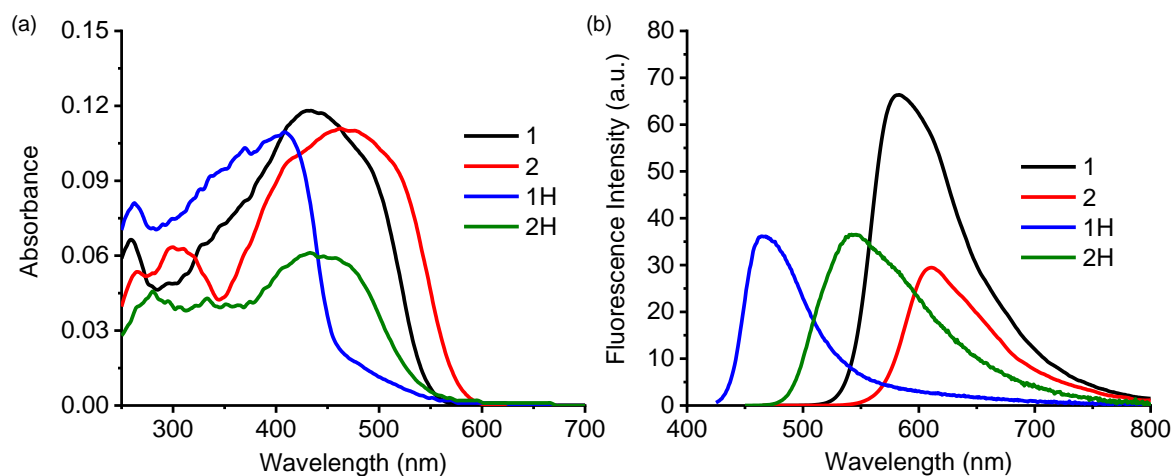


**Fig. S17.** (a) Absorption and (b) emission spectra of **1**, **2**, **1H** and **2H** in the single crystalline state. Excitation wavelength, 430, 465, 408 and 433 nm, respectively.

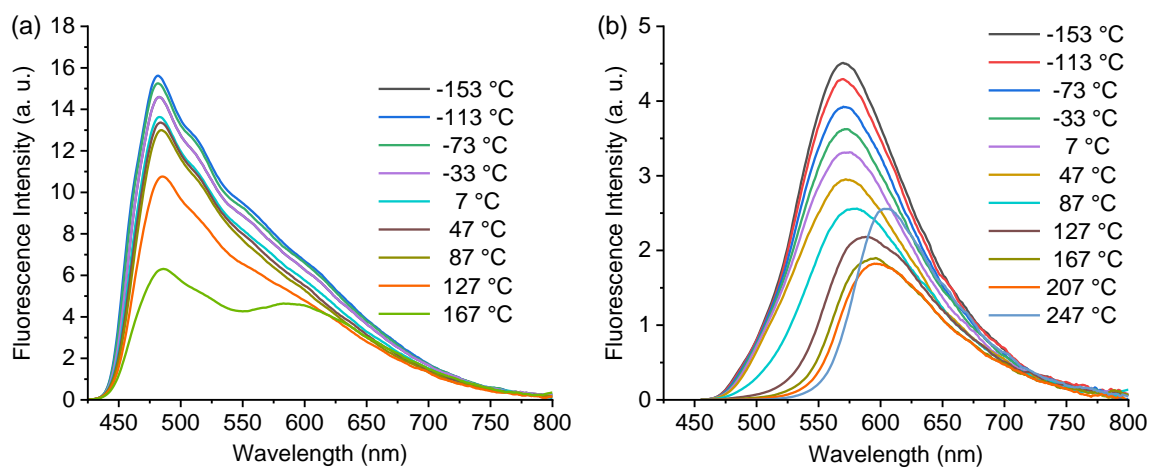


**Fig. S18.** Fluorescence spectra of the crystals of (a) **1H** and (b) **2H** at different temperatures.

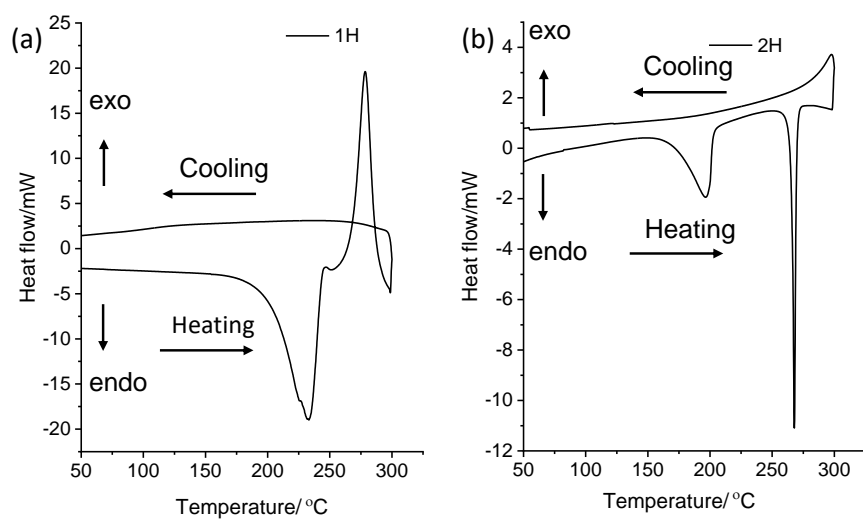


**Fig. S19.** Differential scanning calorimetry curves of (a) **1H** and (b) **2H**. Heating and cooling curves were recorded at a rate of 10 °C/min.

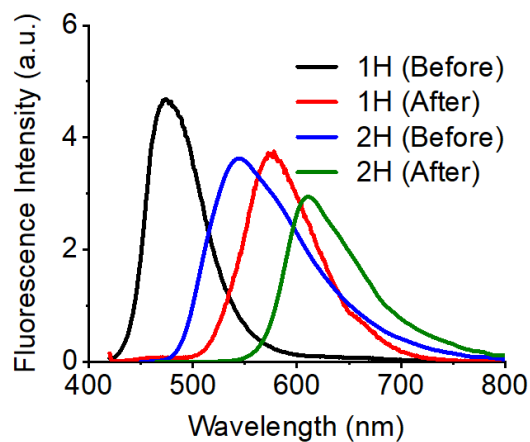


**Fig. S20.** Fluorescence spectra of the crystals of **1H** and **2H** before and after acid release.

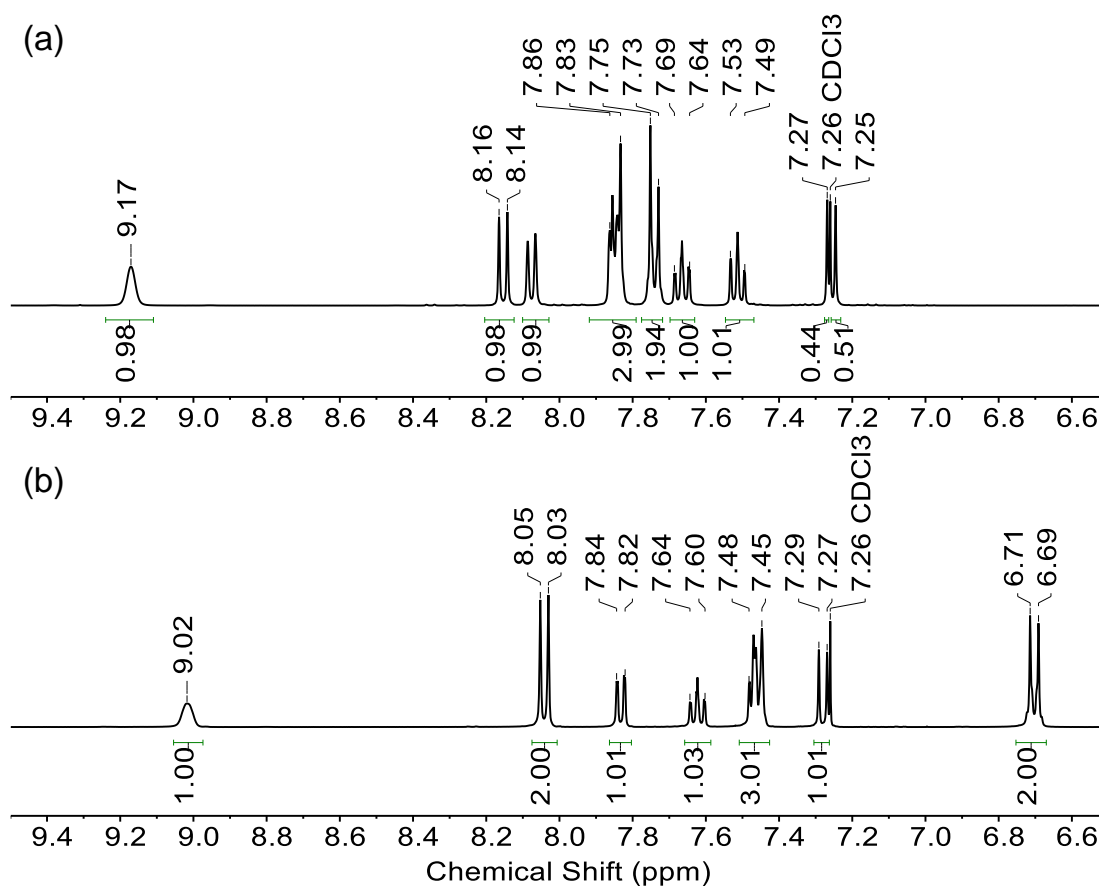


**Fig. S21.** <sup>1</sup>H NMR spectra of **1H** (16.1 mM) in CDCl<sub>3</sub> (a) before and (b) after acid release.



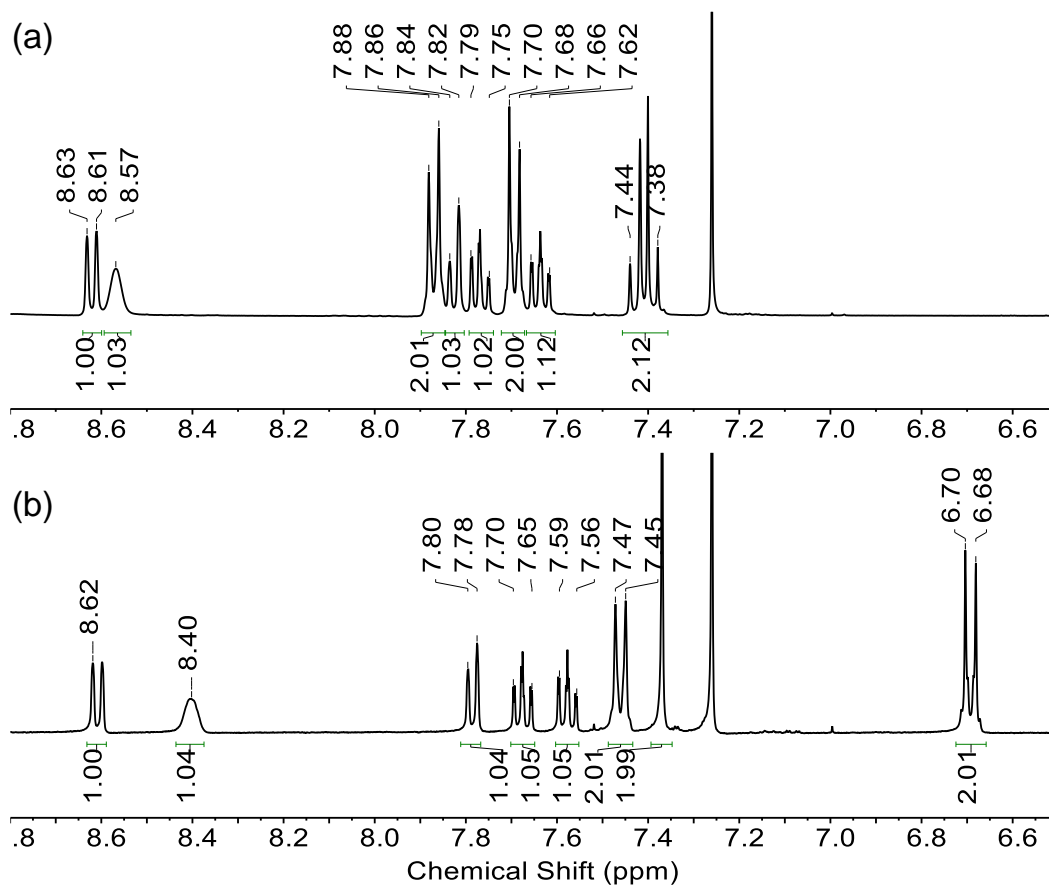


**Fig. S22.**  $^1\text{H}$  NMR spectra of **2H** (12.9 mM) in  $\text{CDCl}_3$  (a) before and (b) after acid release.

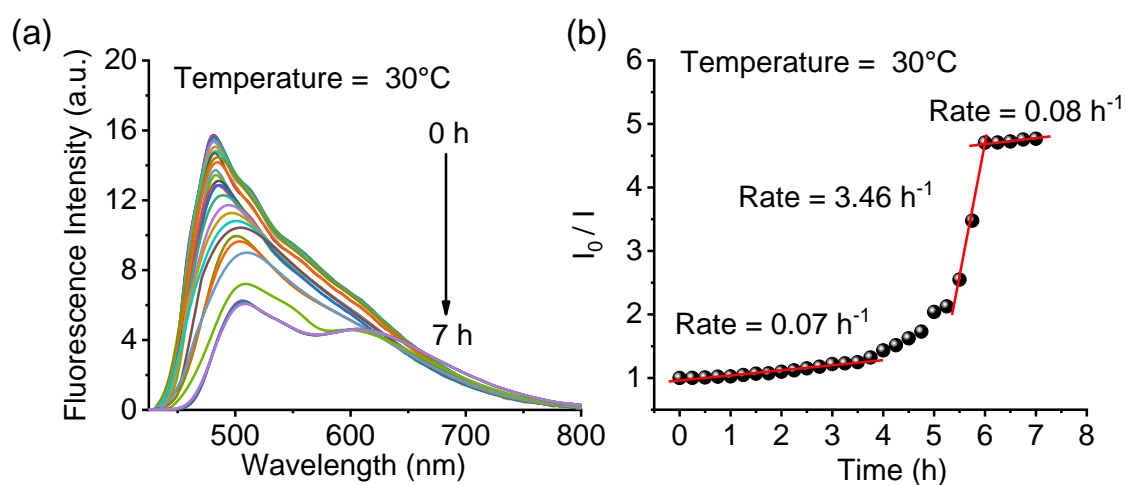


**Fig. S23.** (a) Time dependent emission spectrum and (b) rate kinetics of acid release of **1H** at  $30^\circ\text{C}$  temperature.

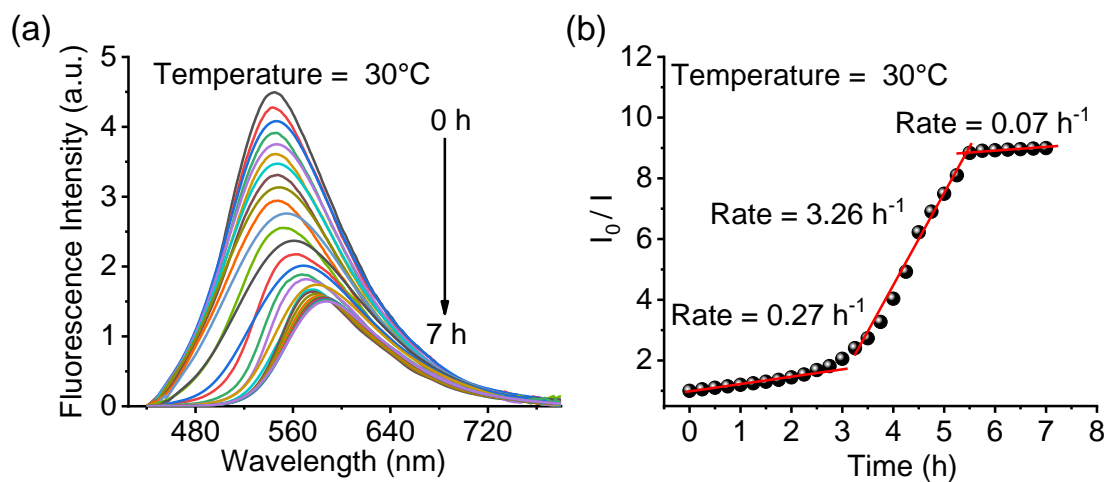


**Fig. S24.** (a) Time dependent emission spectrum and (b) rate kinetics of acid release of **2H** at 30 °C.

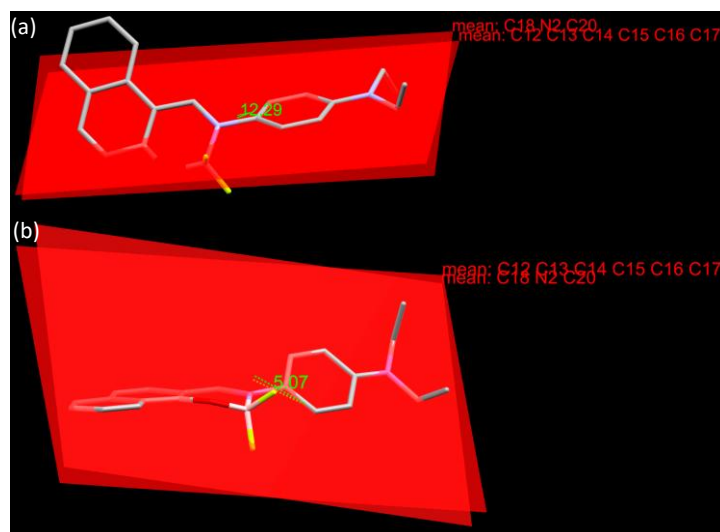


**Fig. S25.** Angle between the plane of phenyl spacer and C18-N2-C20 plane in the crystal packing of (a) **1** and (b) **2**.

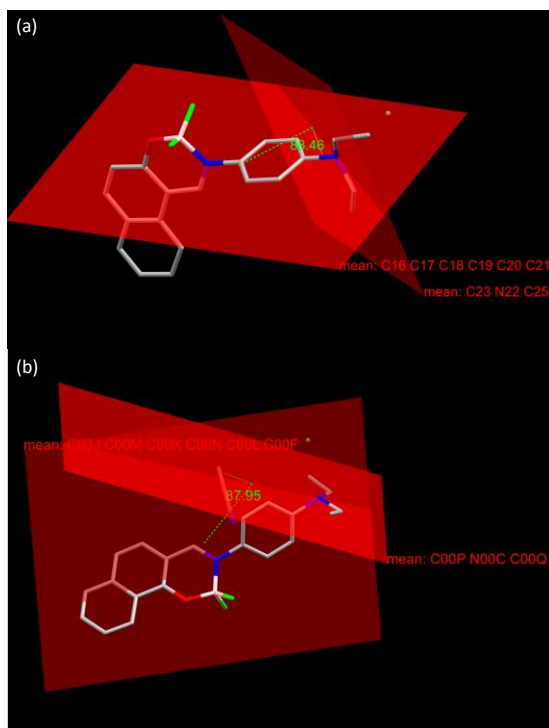


**Fig. S26.** Dihedral angle between C18N2C20 plane and the phenyl spacer in the crystal packing of (a) **1H** and (b) **2H**.

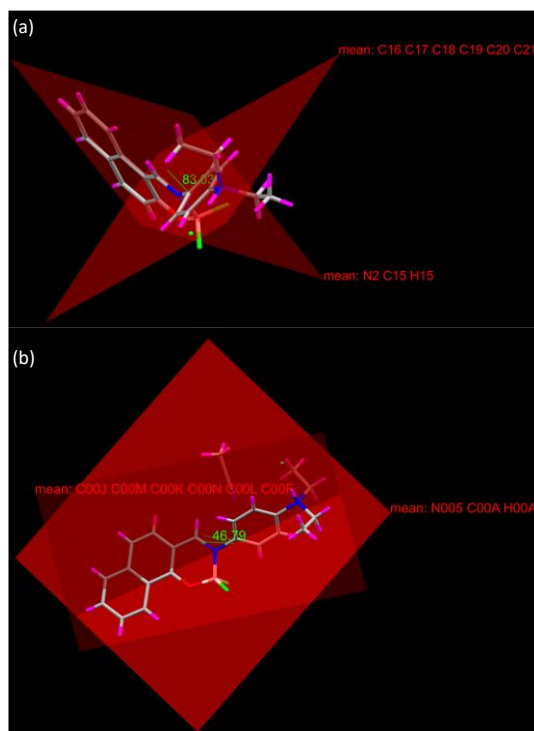


**Fig. S27.** Angle between the phenyl spacer and C11N11H1 plane in the crystal packing of (a) **1H** and (b) **2H**.

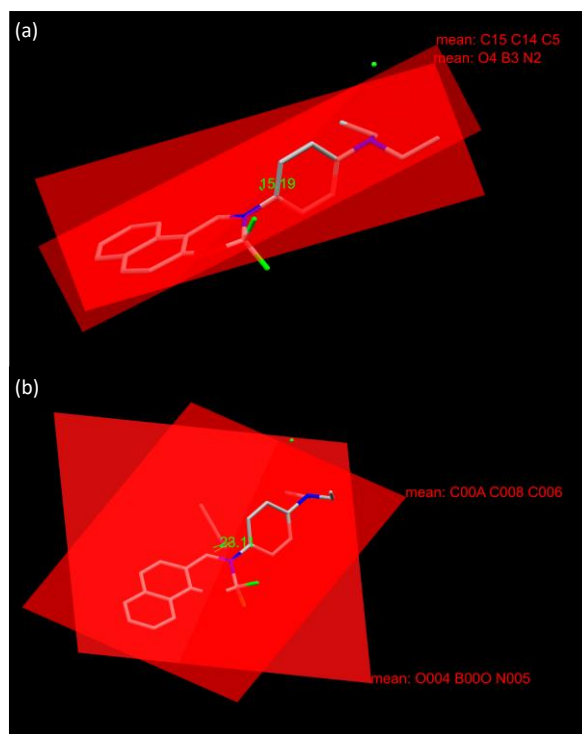


**Fig. S28.** Angle between the planes of O1–B1–N1 and C1–C10–C11 plane in the crystal packing of (a) **1H** and (b) **2H**, respectively.

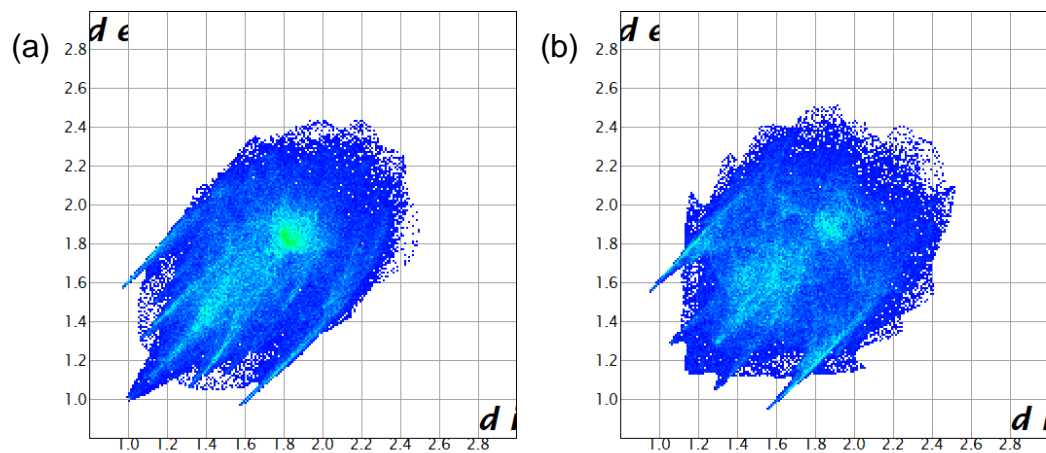


**Fig. S29.** Hirshfeld 2D fingerprint plot of (a) **1H** and (b) **2H**.

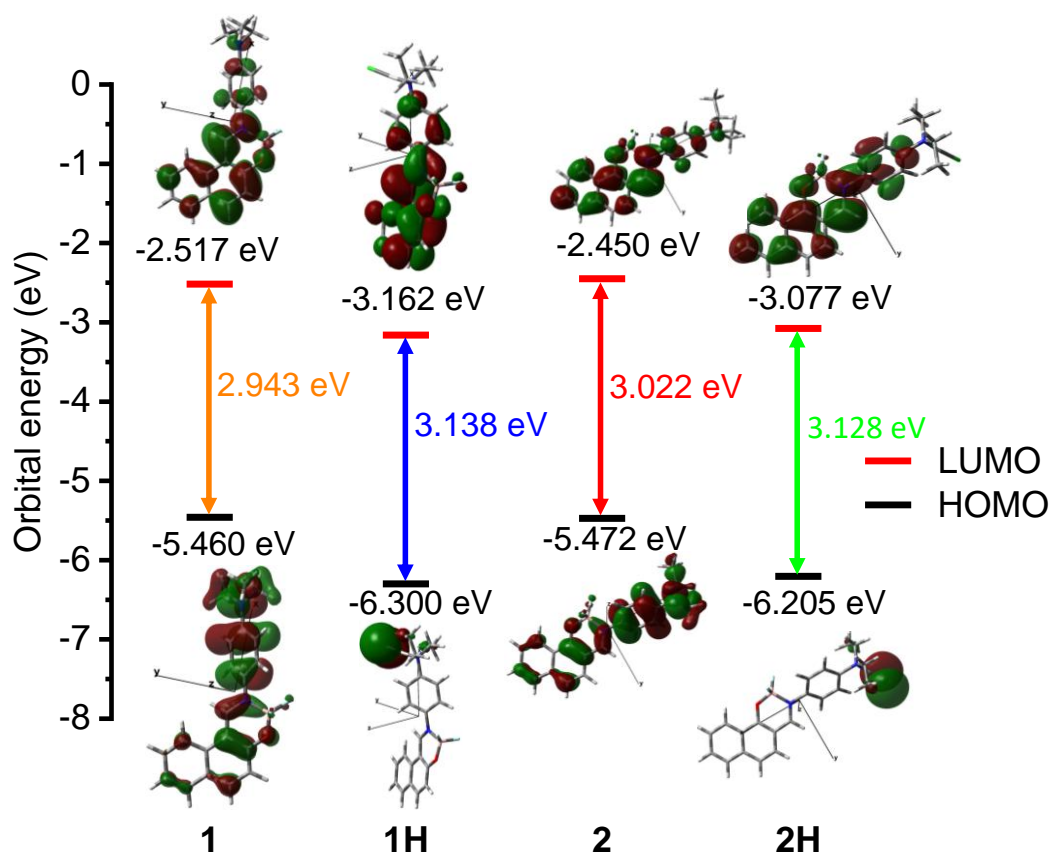


**Fig. S30.** Molecular orbital diagrams and calculated HOMO-LUMO energy levels for **1**, **2**, **1H** and **2H**.

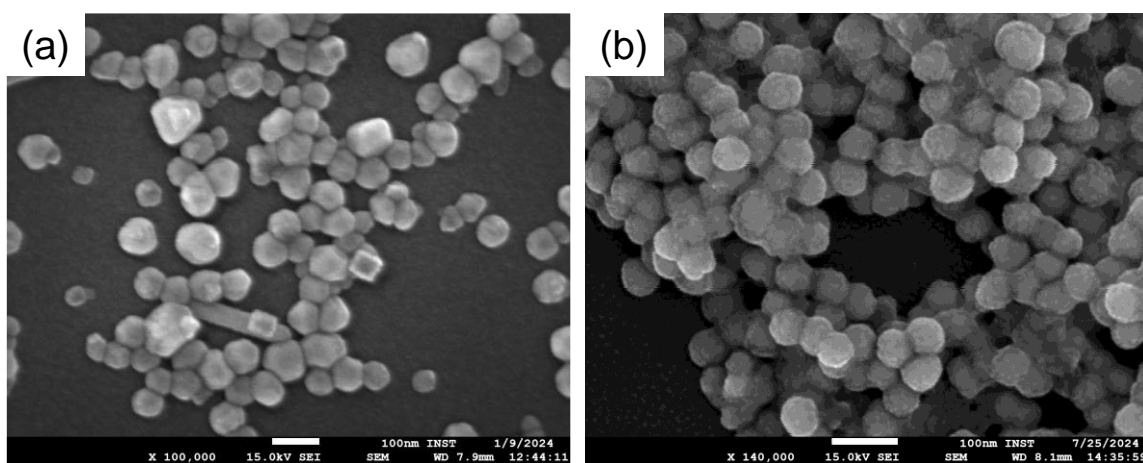


**Fig. S31.** Scanning electron microscopy images of (a) silver and (b) gold nanoparticles. Scale bar is 100 nm.

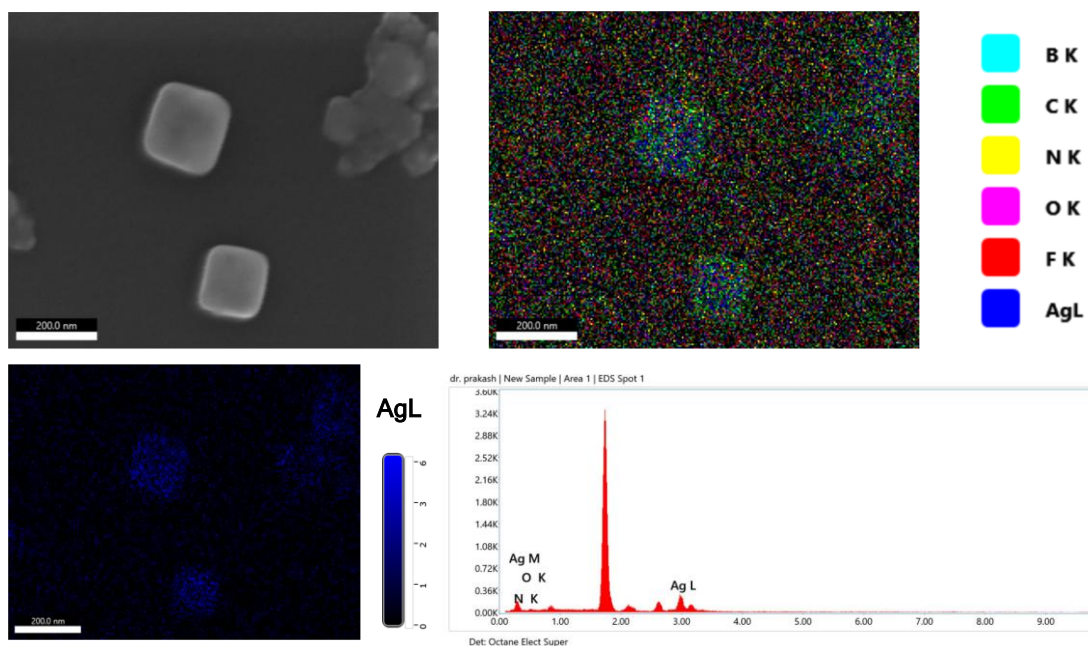


**Fig. S32.** Energy-dispersive X-ray mapping and respective spectrum for silver nanocubes.

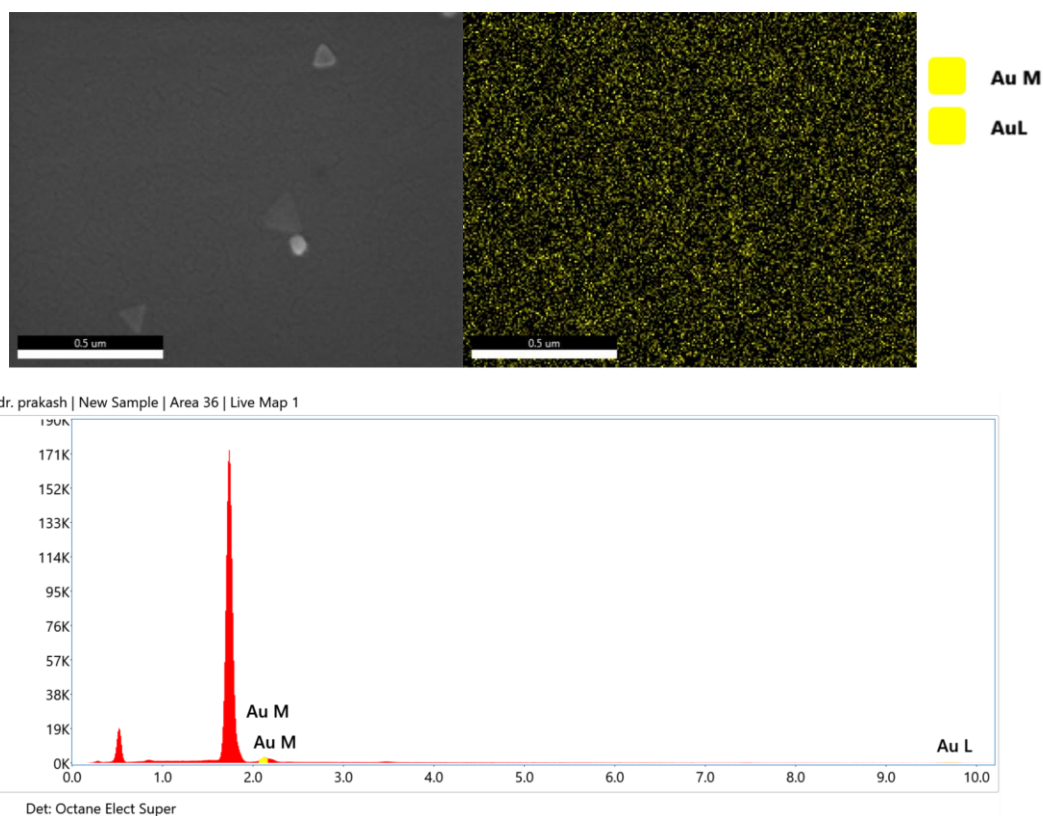


**Fig. S33.** Energy-dispersive X-ray mapping and respective spectrum for gold nanotriangles.

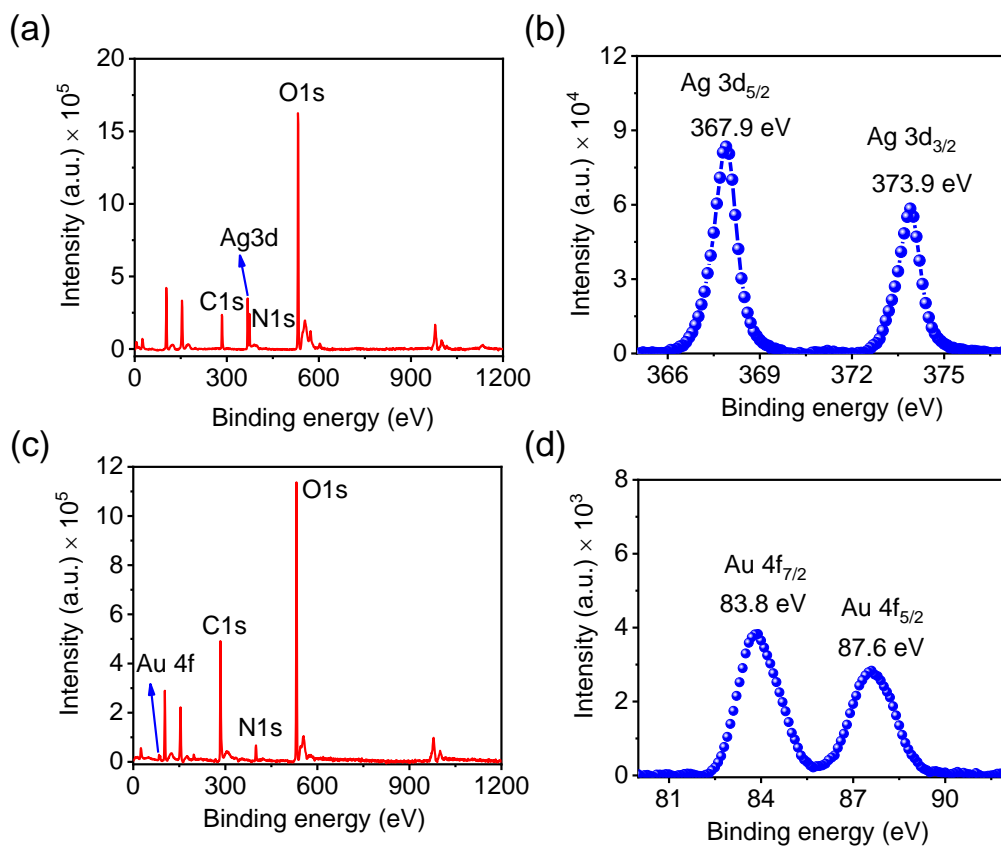


**Fig. S34.** X-ray photoelectron survey spectra of (a) silver nanocubes and (c) gold nanotriangles. Enlarged XPS data of (b) Ag 3d and (d) Au 4f.

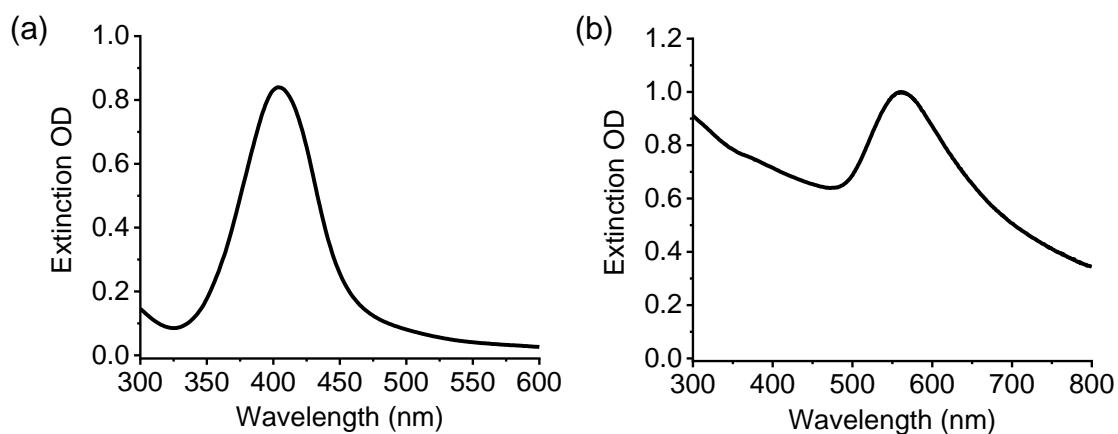


**Fig. S35.** Extinction spectra of (a) silver nanocubes (25 μg/mL) and (b) gold nanotriangles (25 μg/mL).

## References

- 1 I. E. Kareev, I. V. Kuvychko, S. F. Lebedkin, S. M. Miller, O. P. Anderson, K. Seppelt, S. H. Strauss and O. V. Boltalina, *J. Am. Chem. Soc.*, 2005, **127**, 8362–8375.
- 2 O. V. Dolomanov, L. J. Bourhis, R. J. Gildea, J. a. K. Howard and H. Puschmann, *J. Appl. Cryst.*, 2009, **42**, 339–341.
- 3 M. C. Burla, R. Caliandro, M. Camalli, B. Carrozzini, G. L. Cascarano, L. De Caro, C. Giacovazzo, G. Polidori, D. Siliqi and R. Spagna, *J. Appl. Cryst.*, 2007, **40**, 609–613.
- 4 G. M. Sheldrick, *Acta Cryst. C*, 2015, **71**, 3–8.
- 5 M. Woińska, S. Grabowsky, P. M. Dominiak, K. Woźniak and D. Jayatilaka, *Sci. Adv.*, 2016, **2**, e1600192.
- 6 M. J. Turner, J. J. McKinnon, S. K. Wolff, D. J. Grimwood, D. Spackman, D. Jayatilaka and M. A. Spackman, CrystalExplorer 17 (version 17) University of Western Australia 2017.
- 7 M. A. Spackman and D. Jayatilaka, *CrystEngComm*, 2009, **11**, 19–32.
- 8 M. E. Vázquez, J. B. Blanco and B. Imperiali, *J. Am. Chem. Soc.*, 2005, **127**, 1300–1306.
- 9 S. Mukherjee, A. Chattopadhyay, A. Samanta and T. Soujanya, *J. Phys. Chem.*, 1994, **98**, 2809–2812.